Research Article | Vol. 12, No. 10 / 1 Oct 2021 / Biomedical Optics Express 6601
Biomedical Optics EXPRESS

Optoelectronic manipulation of bio-droplets containing cells or macromolecules by active ferroelectric platforms

ANDRÉS PUERTO,[1,*] JOSÉ L. BELLA,[2] CARMEN LÓPEZ-FERNÁNDEZ,[2] ANGEL GARCÍA-CABAÑES,[1,3] AND MERCEDES CARRASCOSA[1,3]

[1]*Departamento de Física de Materiales, Universidad Autónoma de Madrid, c/ Francisco Tomás y Valiente, 7, 28049 Madrid, Spain*
[2]*Departamento de Biología, Universidad Autónoma de Madrid, c/ Darwin, 2, 28049 Madrid, Spain*
[3]*Instituto Universitario de Ciencia de Materiales Nicolás Cabrera, Universidad Autónoma de Madrid, c/ Francisco Tomás y Valiente, 7, 28049 Madrid, Spain*
[*]*andres.puerto@uam.es*

Abstract: Photovoltaic optoelectronic tweezers are a useful platform with many applications in optical manipulation and nanotechnology. They are based on electrical forces associated with the bulk photovoltaic effect presented by certain ferroelectric crystals, such as Fe doped lithium niobate. This manipulation technique has experienced huge developments in recent years, although its use in biology and biomedicine is still scarce. Recently, a novel strategy has been reported that extends the platform capabilities to the manipulation of polar droplets, such as water and aqueous bio-droplets, promising great potential for biological applications. In this work, we are taking this challenge, addressing the manipulation of cells and macromolecules contained inside the droplets by optoelectronic ferroelectric platforms. On the one hand, experiments of photoelectric induced migration of DNA and sperm droplets have been successfully developed and the corresponding droplet dynamics have been analyzed in depth. From this analysis, parameters of the biomaterial such as its concentration and its electrical charge have been evaluated, showing the sensing capabilities of the platform. In fact, the charge of sperm cells has been demonstrated to be negative, and the relative sperm concentration of the samples determined. On the other hand, experiments on the light-induced merging of two droplets have been carried out. Specifically, sperm droplets are mixed with droplets containing acridine orange, a convenient dye for visualization purposes. The spermatozoa become clearly visible in the final droplet through fluorescence imaging. The results point out the multiple possibilities of application of the optoelectronic ferroelectric platform in biology and biomedicine including the development of "lab on a chip" devices. Hence, these capabilities introduce these platforms as an efficient tool in biotechnology.

1. Introduction

Manipulating water and aqueous bio-droplets is an important issue in biomedicine and biotechnology [1–4]. For this goal electrical methods are an efficient and very consolidated option [5–7]. In fact, microfluidic devices with integrated arrays of electrodes have been developed to manipulate very efficiently individual droplets, independently of each other [8–10] for "lab-on-chip" applications. An interesting and flexible alternative are optical methods such as optical tweezers [11,12] and optoelectronic tweezers [13,14]. Pure optical techniques have been used to trap liquid aerosol droplets [15,16], but for manipulating bio-elements and particularly living materials, the light intensities typically used could hurt these bio-components [17,18]. As optoelectronic tweezers use lower intensities, they allow working more safely being an excellent option to

#435730 https://doi.org/10.1364/BOE.435730
Journal © 2021 Received 8 Jul 2021; revised 11 Sep 2021; accepted 21 Sep 2021; published 30 Sep 2021

Biomedical Optics EXPRESS

handle biomaterials [19]. Typical optoelectronic tweezers are based on a platform essentially made up of a photoconductor substrate connected to an AC external electric field. They generate large forces able to massively manipulate particles and cells [20] and single aqueous droplets in microfluidic platforms [21–24]. An alternative kind of optoelectronic tweezers combining the advantages of optical and electrical methods, the so called photovoltaic optoelectronic tweezers (PVOT), has been also proposed [25,26]. PVOT have demonstrated to be a remarkable tool for the manipulation, trapping, and patterning of a variety of micro- and nano- particles [27,28]. These tweezers are based on the bulk photovoltaic (PV) effect presented by some ferroelectric crystals such as Fe doped lithium niobate (LN:Fe) for which the effect is particularly strong. Only induced by illumination an electric field is generated inside the crystal that extends outside as an evanescent field. Evanescent electric field values as high as 200 kV/cm have been recently measured very close to the crystal surface [29]. These fields allow the manipulation of micro- and nano-objects by electrophoretic or dielectrophoretic forces when the objects are immersed in a non-polar medium such as tetradecane, hexane or heptane [30–32] or simply in air [26,33]. The main strengths and advantages of the method are: 1) The simplicity of the platform that basically needs the nude photovoltaic substrate and the light source, without external power supplies or any previous processing for electrode deposition on the substrate. 2) The all optical control and its versatile electric field reconfiguration capabilities. 3) The possibility to use low light intensities or to separate the illumination from the region in which the particles/objects are manipulated (for instance, using a planar optical waveguide as active substrate as reported by Jubera *et al.* [34]. 4) The possibility of object manipulation just after illumination [27,35] because, usually, the electric field remains in dark.

Recently, PVOT have been also applied to handle single droplets and it has been very successful when acting on non-polar droplets [36–39]. The manipulation of water and aqueous droplets is much more difficult and only very recently some progress on the subject has been reported [40–42]. However, this is a key and challenging task because it opens the door to applications in biomedicine and biotechnology. This kind of applications have been envisaged by several authors [38,39,42] but no real demonstration has been provided so far. In this direction our group has very recently proposed [35] a novel and successful strategy where aqueous droplets are manipulated in paraffin oil and hanging from the interface oil-air. Using it, a variety of actions on aqueous droplets, e.g., guiding, trapping at the $LiNbO_3$ substrate, merging, and splitting have been demonstrated. Furthermore, preliminary results demonstrating the possibility of manipulating bio-droplet such as DNA aqueous solutions are reported.

The aim of this work is to definitely demonstrate the successful operation of photovoltaic optoelectronic platforms for the manipulation of bio-droplets, opening the way their use for to biomedical applications. Moreover, then novel optofluidic platform can exploit the advantages of this kind of optoelectronic method cited above. The optoelectronic-induced migration of sex cells (sperm) and biological macromolecules (DNA) are addressed using the hanging droplet strategy [35]. The dynamics of the droplets will be analyzed in detail identifying the physical mechanisms involved. Moreover, two kinds of biological/biomedical applications are investigated: i) sensing the charge and concentration of the droplet biological content. ii) Sperm visualization/imaging by light-induced merging of the sperm droplet with an appropriate fluorophore contained in a second droplet. A discussion on the mechanisms allowing the manipulation of polar droplets and on the impact of the technique on applications in optofluidics and biomedicine is also included.

2. Photovoltaic optoelectronic platforms for droplet manipulation

The main elements of the photovoltaic optoelectronic platforms (POP) are the PV substrate and the light source illuminating it. In addition, either for the case of particle or droplet manipulation, these micro- or nano-objects are usually suspended in a non-polar liquid.

Biomedical Optics EXPRESS

The active mechanism is the bulk PV effect. This effect arises from asymmetric excitation of electrons [43] from the impurities (Fe in LN:Fe) giving rise to an electric current along the ferroelectric polar axis (c-axis). As a consequence, a light-induced charge appears at the crystal surfaces normal to the c-axis, generating a bulk PV electric field [44]. A schematic of the POP is provided in Fig. 1 showing the photo-induced charge distribution and electric field lines generated inside and outside of the ferroelectric plate.

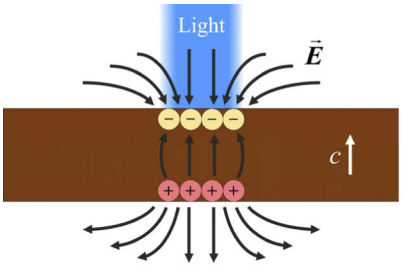

Fig. 1. Schematic of LN:Fe plate under illumination indicating the ferroelectric polar axis, called c-axis, normal to the active surfaces (z-cut substrate). The black arrows represent the electric field lines. The yellow and red circles are negative and positive charges, respectively.

The electric field $\mathbf{E}$ extends to the surroundings of the plate and can act on nearby charged and neutral micro- or nano-particles through electrophoretic and/or dielectrophoretic forces [27,45]. Electrophoretic (EP) forces, $\mathbf{F}_{EP}$, are simply expressed by:

$$\mathbf{F}_{EP} = q\mathbf{E} \tag{1}$$

where q is the total charge of the object. In turn, the expression for the dielectrophoretic (DEP) forces, $\mathbf{F}_{DEP}$, under non oscillating electric fields (as the PV fields) for the relevant case of spherical objects, such as the droplets investigated here, is:

$$\mathbf{F}_{DEP} = (\mathbf{p}\cdot\bar{\nabla})\mathbf{E} = \alpha_p\bar{\nabla}(\mathbf{E})^2 \tag{2}$$

$\mathbf{p}$ being the dipolar momentum of the object induced by the evanescent photovoltaic field $\mathbf{E}$, and α_p the polarizability that for spherical objects can be written as [45]:

$$\alpha_p = 2\pi r^3\varepsilon_0\varepsilon_m\frac{\sigma_p-\sigma_m}{\sigma_p+2\sigma_m} \tag{3}$$

r being the radius of the particle or droplet, ε_m is the dielectric permittivity of the medium containing the particles (usually air or a non-polar liquid), and σ_m and σ_p the conductivities of this host medium and particles, respectively. Note that when σ_p is much larger than σ_m (as it occurs for aqueous droplets immersed in oil), the polarizability can be simplified to:

$$\alpha_p \simeq 2\pi r^3\varepsilon_0\varepsilon_m \tag{4}$$

that only depends on the dielectric constant of the surrounding medium ε_m and the particle radius r.

It is worthwhile mentioning that when a particle has no charge it undergoes only a DEP force but when it is charged EP and DEP forces contribute to the net force as discussed in Ref. [46] and the EP force only dominates if the amount of charge is high enough [47].

When the objects to be manipulated are biomaterials, some additional remarks have to be made: 1) Most bio-objects are solved in aqueous media. However, water screens the crystal electric fields preventing the bio-object manipulation. 2) When water droplets contact with the

Biomedical Optics EXPRESS

optoelectronic platform, they become immobilized on the LN:Fe surface due to a high wettability even enhanced by the PV electric fields [40].

The strategy to overcome these problems, proposed in Ref. [35], is manipulating bio-objects inside aqueous droplets suspended in a non-polar host medium (a layer of paraffin oil). Moreover, the droplets are separated from the ferroelectric surface by keeping them hanging from the interface between air and paraffin (see Fig. 1(b)) due to surface tension effects that are described in detail in Refs. [48,49]. This way, wettability effects are avoided. With this strategy several successful manipulation schemes, light–induced guiding, splitting, and merging, have been demonstrated for water droplets with promising results. Here, we will exploit this approach to handle the bio-droplets.

3. Experimental method

The experimental method used in this work is similar to that described in detail in Ref. [35] and has been schematized in Fig. 2. The optical part of the experimental system is shown in Fig. 2(a). The optical glass cuvette containing the PV substrate is located on the mobile platform, where the lens objective focused the laser beam on the active surface of the substrate. The process is recorded by a top and a lateral CMOS camera. White light coming from the bottom of the system is employed for visualization purposes.

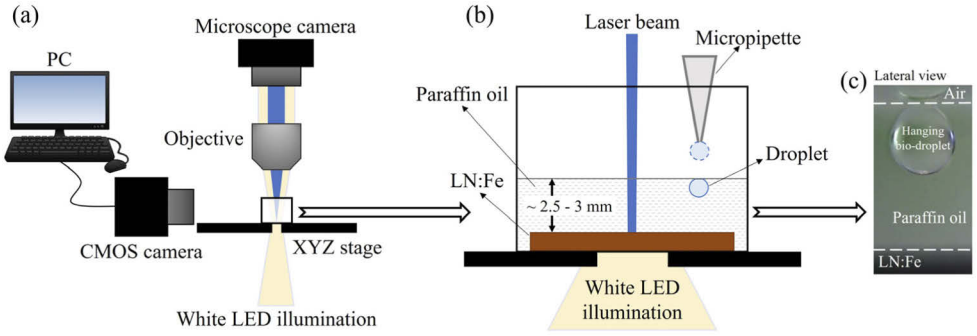

Fig. 2. (a) Schematic of the optical system used in the experiment for observing and controlling the droplet manipulation process. (b) Detail of the glass cuvette with the photovoltaic substrate on the bottom covered by the paraffin oil. (c) Photograph of a bio-droplet (containing DNA) hanging at the interface air-paraffin oil. Dashed lines indicate the boundaries between air-paraffin and paraffin-LN:Fe.

As PV substrate, we have used 1 mm thick z-cut LN:Fe crystal plates with a ~0.1% wt of Fe impurities content. As shown in Fig. 2(b), the active PV plate is covered with a paraffin oil layer of about 2.5-3 mm that it is used as non-polar host medium. Before turning the laser beam on, the droplet sample is carefully deposited with a micropipette over the paraffin oil layer. The droplet stays hanging at the interface air-paraffin oil by surface tension forces [48,49], as it is shown in Fig. 2(c), where it can be easily manipulated. Here, we will manipulate aqueous droplets containing DNA and sperm with volumes less than 1 μL. Water droplets of equal volumes has been also used as reference.

To activate properly the photovoltaic optoelectronic platform, a laser diode single emission at $\lambda = 488$ nm has been selected because it matches with the optical absorption band peak associated with the ionization of Fe^{2+} in LN:Fe crystals [50]. The laser beam is focused with a long-work distance objective (5×, NA=0.14, working distance=34.0 mm) on the surface substrate with a

Biomedical Optics EXPRESS

Gaussian intensity profile given by the expression:

$$I(r) = I_p \exp\left(\frac{r^2}{2\sigma_G^2}\right) \tag{4}$$

being I_p the intensity peak, and σ_G the standard deviation of the Gaussian profile. Specifically, in this work we use a $I_p = 8$ W/cm^2 and a spot diameter ($4\sigma_G$) of 480 μm.

4. Bio-droplet migration under light-induced electrical forces

In this section, we describe experiments to investigate bio-droplet migration along the air-oil interface by the action of PV fields controlled by light. In all these experiments, the paraffin oil layer thickness is 2.7 mm. This value is large enough to avoid that the hanging droplet fall and trap on the substrate when approach to the illuminated region. The droplet volume is 0.8 μL along the work. All droplets start to move around 1.5 - 2 mm from the illuminated region.

First, droplets of DNA solution samples are pipetted on the paraffin surface, and they become hanging from the interface air-paraffin. Then, the laser beam is focused on the substrate at a certain distance from the droplet position to generate the electric field inside the ferroelectric crystal that extends to the paraffin oil. As expected from the results of previous work [35], we get a droplet motion along the interface approaching to the vertical of the substrate region illuminated by the laser beam. Finally, it stops at the illuminated region. The droplet trajectory is roughly rectilinear as it can be inferred from the lateral and top views of the droplet migration. An example is shown in Fig. 3 (corresponding to Visualization 1 included in the Supplement 1) for an initial distance d from the droplet to the light beam of $d = 2$ mm. Figure 3(a) by the lateral camera and Fig. 3(d) by the top camera correspond to the initial droplet position just before illumination ($t = 0$ s). Figure 3(b) and Fig. 3(e) show an intermediate position along the droplet trajectory for $t = 10$ s taken by the lateral and the top view, respectively. And Fig. 3(c)

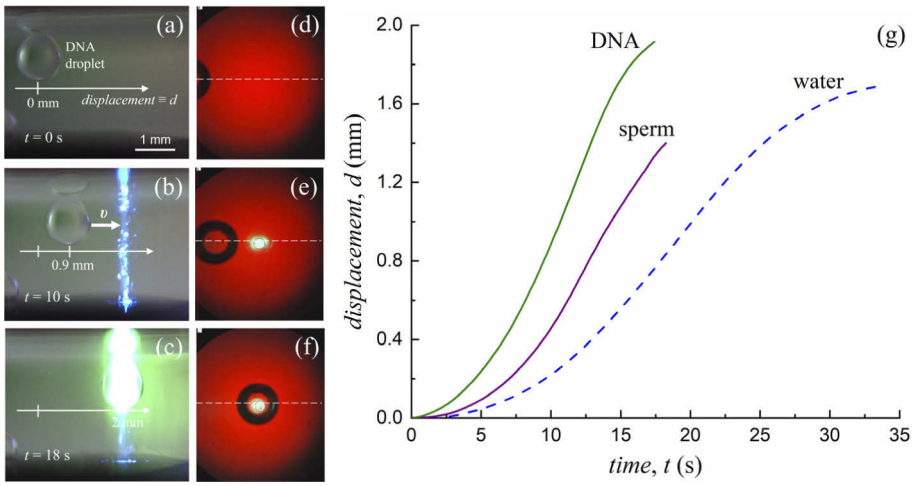

Fig. 3. (a-c) Lateral view and (d-f) top view photographs taken by the corresponding CMOS camera of the DNA droplet migration. (a) and (d) Bio-droplet deposited at the interface paraffin-air just before illumination; (b) and (e) photograph of the droplet at $t = 10$ s during its motion approaching the illuminated substrate region; and, (c) and (f) DNA droplet arriving at the illuminated region. (g) Time evolution of the droplet displacement d during migration for three kinds of droplets used in the experiment: DNA (green line), diluted sperm (purple line), and water (dashed blue line) as reference. At $t = 0$ s the laser is turned on and the movement starts.

Biomedical Optics EXPRESS

and Fig. 3(f) correspond to the final position. Finally, to fully characterize the droplet dynamics, Fig. 3(g) shows the DNA droplet displacement d as a function of time obtained from the data recorded by the video-camera. The video-camera data has been extracted using the free software "Tracker". Since the lateral camera has a larger field of view than the top camera, as it can be observed comparing Figs. 3(a) and 3(d), the droplet dynamic data has been obtained from the videos taken by this camera. The software provides one data (i.e. in our case a droplet position) per video frame. The manipulation technique should be effective for a wide variety of bio-droplets. To illustrate it, in addition to DNA macromolecules, bio-droplets containing human sperm cells has been tested. The previous experiment has been repeated under the same experimental conditions with droplets of sperm diluted in water of the same volume (0.8 µl). Deionized water droplets have been also probed for reference. The corresponding kinetic curves $d(t)$ for sperm and water are also displayed in Fig. 3(d). One can see that the three kinetics are similar although the velocity is markedly higher for the bio-droplets.

5. Analysis of the droplet dynamics

In order to understand and to better control the horizontal droplet motion, it is worthwhile to analyze the dynamics. To this end, starting from the curves $d(t)$ of Fig. 3(d), we have calculated the time evolution of the droplet velocity $v(t)$ and acceleration $a(t)$, by making the corresponding derivatives. Finally, from the acceleration multiplied by the mass we obtain the net horizontal force $F_N(t) = ma(t)$. In Fig. 4(a) the time evolution of the obtained droplet velocity $v(t)$ and net force $F(t)$ (see inset) has been plotted for the three droplets. One can see that the maximum velocities are in the range of hundreds of µm/s although the bio-droplets reach values about a factor 2 greater than water. The net force, shown in the inset of Fig. 4(a), rapidly decreases initially reaching values of the order of a few pN.

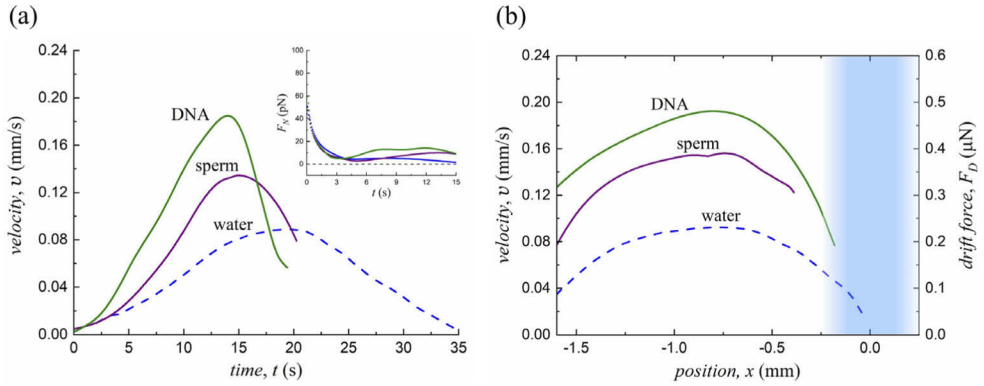

Fig. 4. (a) Time evolution of the velocity for the three kinds of droplets: DNA (green line), diluted sperm (purple line), and water (dashed blue line) as reference. In the inset it is represented the net force vs time until $t = 15$ s. (b) Droplet velocity (left axis) and drift force (right axis) as a function of droplet position with regard to the light beam which is centered at x=0 mm and drawn as a blue fringe in the graph.

To discuss this behavior, let us analyze the main forces acting on the horizontal motion of the droplet. In the previous work [35], this analysis has been preliminary discussed for a water droplet. The motion started with a horizontal dielectrophoretic drift force F_D that very soon was quasi-balanced by the friction force F_f appearing during the motion inside the paraffin oil, a rather viscous liquid. So, the net force on the droplet F_N=F_D –F_f. This model can be also applied to the dynamics of the bio-droplet since the net force decreases rapidly in the first two seconds. Hence, for $t > 2$ s, $F_D \cong F_f$. Moreover, as the droplets are roughly spherical the friction

Biomedical Optics EXPRESS

force can be approximately described by the Stokes force:

$$F_f = F_{Stokes} = 6\pi v\eta r \approx F_D \tag{5}$$

where η is the liquid viscosity ($\eta = 0.23$ Pa·s in the paraffin oil used). This force can be calculated from the velocity experimental data taking into account that $r = 0.6$ mm ($V_{droplet} = 0.8$ µL). Note that expression (5) allows measuring the friction and, importantly, the drift force from the droplet velocity.

It is worthwhile noting that the drift force, originated by the evanescent PV fields, varies with the distance to the illuminated region. In Fig. 4(b), the position dependence of the velocity (left axis) and the horizontal drift force $F_D \approx F_f$ (right axis) are shown. Note that the same curve represents both magnitudes because they are proportional. In fact, the right axis is given in force units. The curves initially grow, and they have a maximum still at a certain distance to the light beam where the horizontal electric field component start to decrease and the vertical component to increase.

At this point and taking into account that the experimental conditions (including the droplet volume) are the same for the three cases (water, sperm and DNA), one can wonder the origin of the substantially higher velocity of bio-droplets with regard to water. Initially, one can think its origin is a different polarizability (see Eq. (3)) but this is not the case because the paraffin is a nonpolar liquid with a negligible conductivity with regard to that of water or, even more, with regard to aqueous bio-droplets. Hence, the droplet polarizability is simply $\alpha_p = 2\pi r^3 \varepsilon_0 \varepsilon_m$ equal for the three droplets. Another possible origin could be that bio-droplets are charged instead of neutral and the drift force has an electrophoretic component (see Section 2). To check this proposal, we have designed a charge test experiment in which each droplet is manipulated exposed to the $+c$ crystal face instead to the $-c$ face used in the experiments of the Section 4. As it can be seen in the scheme of Fig. 1, the $-c$ face is charged positively whereas the $+c$ face is charged negatively. So, if there is a high enough electrophoretic component in the experiments of Section 4, its sign should change when the crystal face is changed i.e.:

$$F_D = F_{DEP} + F_{EP}, \text{ for } -c \text{ face} \tag{6a}$$

$$F_D = F_{DEP} - F_{EP}, \text{ for } +c \text{ face} \tag{6b}$$

Then, we have made the corresponding experimental tests, exposing the bio-droplets to both, the $+c$ and $-c$ crystal faces, keeping the rest of experimental parameters fixed. The results

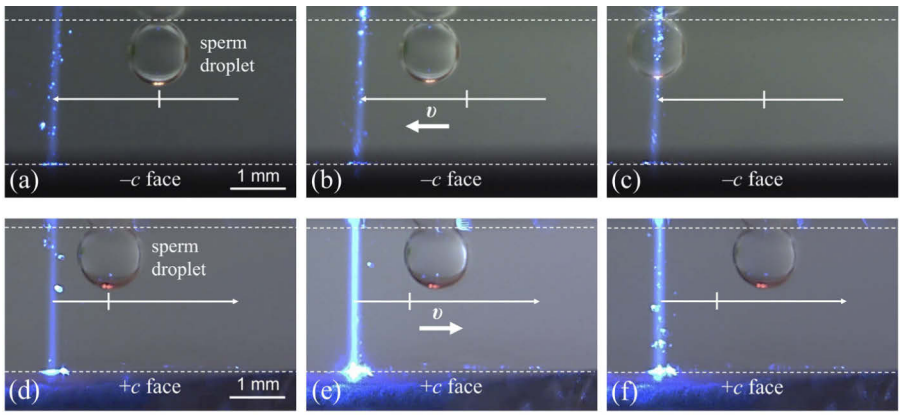

Fig. 5. Photographs taken by the CMOS lateral camera of the sperm droplet migration process: Bio-droplet exposed to (a-c) the $-c$ face and to (d-f) the $+c$ face.

Biomedical Optics EXPRESS

are illustrated in Fig. 5 (and Visualization 2 in the Supplement 1), for a sperm sample. They show that, at difference with the $-c$ face (Fig. 5(a)-(c)) used in previous experiments, in the $+c$ face charged negatively, the droplets are repelled from the illuminated crystal region moving away under a repulsive horizontal drift force. A similar behavior is obtained for DNA droplets. These experiments confirm the existence of an electrophoretic force component acting on the bio-droplets that is larger than the DEP force. In turn, this implies that bio-droplets are charged, and the sign is negative because they are attracted to the positively charged face and repelled to the negative one [51]. On the other hand, the behavior of the water droplet is the same with both faces corroborating that, as previously reported [35], it is neutral and so, it only undergoes a DEP force. In summary, PVOT are able to detect the charge of the manipulated objects. At difference with water droplets, DNA and sperm droplets are negatively charged and the additional attractive electrophoretic force component explains their faster kinetics in the experiments of Section 4.

6. Applications

6.1. Sensing the biomaterial concentration

In this section, we have investigated the influence of sperm concentration on the droplet kinetics. To this end, the migration dynamics of three aqueous droplets A, B, C with the same volume but with decreasing sperm content has been studied. The experimental conditions of the ferroelectric platform are the same of Section 4. The results for the kinetic curves $d(t)$ are shown in Fig. 6(a) (solid lines) together with that of a water droplet (dashed blue line) for reference. It is observed that the droplet motion becomes faster as the sperm concentration increases. This can be better seen in the Fig.6b where the velocity (left axis) as a function of the position with regard to the center of the light beam was shown. As the velocity is proportional to the drift force, we have introduced a second vertical axis, on the right, quantifying the force. The curves maxima are located around the same point in all the cases because it should be essentially determined by the horizontal PV field component only depending on the PV crystal. The higher drift force for larger sperm concentration is easily explained because higher concentration must imply a higher droplet charge and so, a larger electrophoretic force component.

In Fig. 6(c), the maximum velocity v_{max} (left axis) and the maximum force (right axis) for each droplet has been plotted versus the sample sperm concentration C (black squares). Note that we have also included the case of pure water (C=0). The points show a linear dependence that can be used to determine unknown sperm concentrations by simply detecting the velocity maxima of its migration curve $d(t)$. In other words, one can take advantage of the kinetic curves or simply of the velocity maxima as a spermatozoa concentration sensor.

To check the sensing performance, a new sample that was labelled as oligospermic (sample with unknown but very low sperm concentration) has been analyzed by a droplet migration experiment with the same experimental conditions than the previous ones. The corresponding motion curve is also displayed in Fig. 6(a) with a pink dashed line. As expected, it appears between the kinetics of water and that of the sample with lowest sperm concentration. With the measured maximum velocity and using the calibration straight line of Fig. 6(c), (a) value of 10×10^6 spermatozoa/mL has been obtained. In fact, this measured value is in the range usually considered oligospermic, indicated in yellow in Fig. 6(b). Hence, a successful measurement has been achieved, confirming that our method is able to determine the sperm concentration of the samples, providing relevant information for fertility assessment.

6.2. Droplet merging applied to sperm visualization

In this section, another application is investigated based on a different manipulation scheme, e.g., merging of two different droplets. The objective is facilitating the visualization of sperm by mixing the sperm sample droplet with a droplet of an appropriate fluorophore, namely acridine

Biomedical Optics EXPRESS

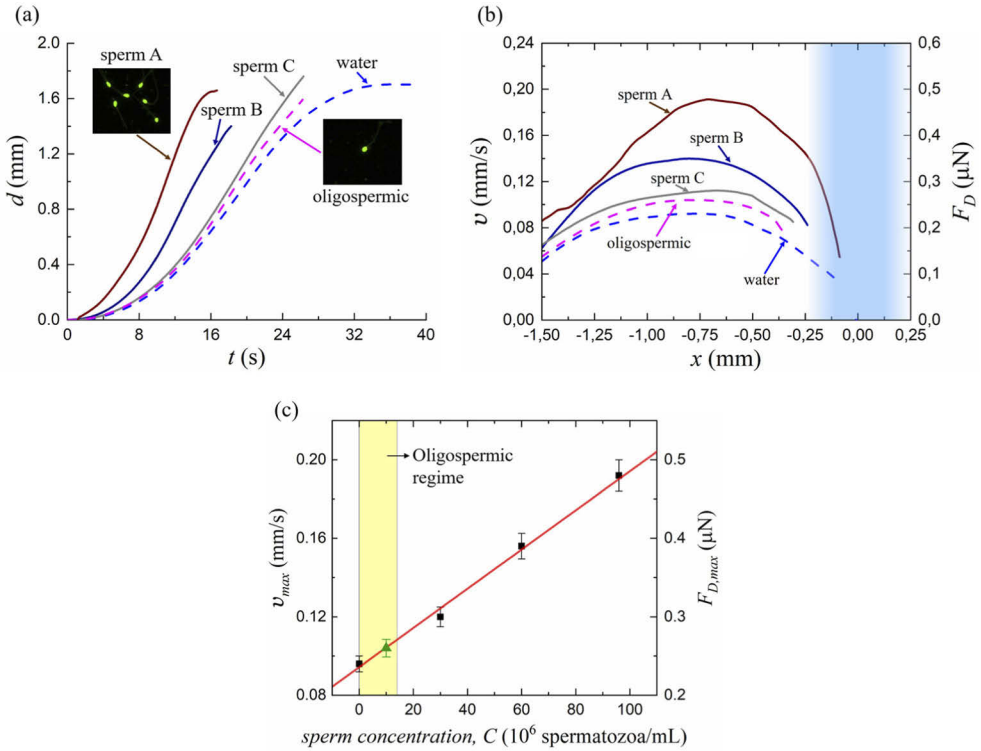

Fig. 6. (a) Time evolution of the displacement d for three different sperm concentration droplets, one water droplet and one oligospermic droplet (see text for details). Fluorescence microscope images of the sperm A and the oligospermic samples are also shown. (b) Dependence of the maximum droplet velocity (left axis) and the maximum drift force (right axis) on the position x regarding to the light beam for all the droplets. The light beam centered at $x = 0$ is drawn as a blue fringe. (c) Graph of the maximum velocity (left axis) and drift force (right axis) as a function of the sample spermatozoa concentration. The red line is a linear fit to the experimental points. The green triangle corresponds to the oligospermic sample. The yellow region indicates the range of sperm concentrations for which a sperm sample is considered oligospermic.

Biomedical Optics EXPRESS

orange (AO). The AO fluorescent dye intercalates into DNA between adjacent base pairs, and it also interacts with phosphate groups outside the DNA [52]. It commonly shows a green fluorescence, used for sperm visualization. In the merging experiment, we will use again the –*c* crystal face because it is necessary to attract the two droplets to the illuminated region. A typical experiment is illustrated in Fig. 7 (and Visualization 3 in the Supplement 1) where a droplet with diluted human sperm (V=1.8 µL), on the left, merges with the droplet of AO (V=0.7 µL). Fig.7a show the initial situation, just at the instant when the laser is turned on. The two droplets approach to the illuminated region (Figs. 7(b) and 7(c)) and contact merging themselves (Fig. 7(d)), resulting in a larger droplet which can be seen in Fig. 7(e) where the AO binds with the DNA. The final droplet has been observed through a fluorescence microscope and a magnified image of the spermatozoa (bright green points) is shown in the inset of Fig. 7(e).

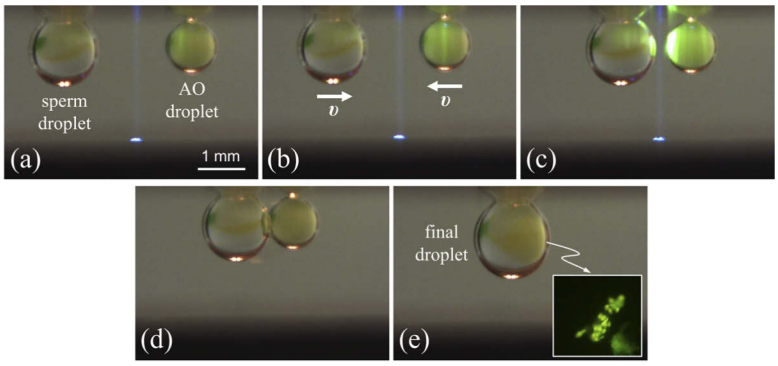

Fig. 7. Sequence of images of the droplet merging process. (a) Sperm droplet (1.8 µL, left) and AO droplet (0.7 µL, right) hanging at the interface paraffin-air just when the laser is turned on. (b), (c) Droplets approaching the illuminated region. (d) The two droplets contact and merge, and the laser is turned off. (e) Final droplet after merging. In the inset, a fluorescence image of the sperm is shown. In the experiment the paraffin layer thickness is $h = 2.5$ mm and the light intensity is $I = 1$ W/cm^2.

Droplet volumes one order of magnitude smaller than those typically used in common genetic essays are employed in our method due to its remarkable capabilities for efficient droplet manipulation and merging. Hence, the method allows a relevant saving of reagents and is well adapted to be implemented in optofluidic lab-on-chip devices. From a general point of view, this droplet merging technique should be well adapted for miniaturizing a wide variety of chemical reactions.

7. Summary and conclusions

Different kind of aqueous bio-droplets, containing DNA macromolecules and sperm cells, have been successfully manipulated by POP. Two main manipulation schemes have been investigated: bio-droplet migration and droplet merging. In the former case, the droplet dynamics has been studied in depth providing much information on the underlying physical mechanisms and the strategy to control the light induced manipulation process. A main finding of this work is that the charge state of the droplet can be measured from the droplet migration behavior. In fact, we have determined that the bio-droplets manipulated in this work are negatively charged whereas water droplets are neutral.

From the point of view of the development and analysis of the photovoltaic platform operation, the droplet migration curves provide a method to measure the drift forces, and from them, the evanescent electric fields generated by the bulk photovoltaic effect. The experimental

Biomedical Optics EXPRESS

determination of these evanescent fields is not easy and only a previous work has reported a method to measure it but only just very close to the crystal surface [29].

The work has been also addressed to the design and demonstration of biological/ biomedical applications of the ferroelectric platform for the first time. On the one hand, the droplet migration kinetics has been used as a biomaterial concentration sensor. In the case of the sperm droplets, this sensing capability is relevant for fertility studies. In fact, the proposed sensor strategy has enabled to detect an oligospermic sample, i.e., a sperm sample with a low concentration of spermatozoa. On the other hand, the technique has been successful applied to sperm visualization by merging the sperm droplet with a suitable fluorophore. Moreover, the presented design allows reducing the involved liquid volumes in at least one order of magnitude with regard to conventional essays. In general, these applications based in ferroelectric platforms acting on bio-droplets should be easily adapted to be implemented in lab-on chip devices.

Globally, the results of this work, definitely demonstrate the possibility of handling aqueous solutions of bio-species by optoelectronic ferroelectric platforms. The technique is flexible and versatile, and it could become an effective and competitive optofluidic tool for multiple applications in fields such as biomedicine, biotechnology, and chemistry.

Funding. Ministerio de Ciencia e Innovación (MICINN) (PID2020-116192RB-I00); Ministerio de Economía, Industria y Competitividad, Gobierno de España (MAT2017-83951-R, PEJ2018-003989).

Acknowledgments. Financial support from Ministerio de Economía, Industria y Competitividad of Spain (MAT2017-83951-R) and Ministerio de Ciencia e Innovación of Spain (PID2020-116192RB-I00) is gratefully acknowledged. A. Puerto acknowledges the funding under Iniciativa de Empleo Juvenil y Fondo Social Europeo (PEJ2018-003989).

Disclosures. The authors declare no conflicts of interest.

Data availability. Data underlying the results presented in this paper are not publicly available at this time but may be obtained from the authors upon reasonable request.

Supplemental document. See Supplement 1 for supporting content.

References

1. M. T. Guo, A. Rotem, J. A. Heyman, and D. A. Weitz, "Droplet microfluidics for high-thoughput biological assay," Lab Chip **12**(12), 2146–2155 (2012).
2. S. Tasoglu, U. A. Gurkan, S. Q. Wang, and U. Demirci, "Manipulating biological agents and cells in micro-scale volumes for applications in medicine," Chem. Soc. Rev. **42**(13), 5788–5808 (2013).
3. L. Pang, J. Ding, X. X. Liu, and S. K. Fan, "Digital microfluidics for cell manipulation," Trends Anal. Chem. **117**, 291–299 (2019).
4. H. Liu and Y. Fei, "Recent advances in digital biomolecule detection with single copy sensitivity," Biosens. Bioelectron. **177**, 112901 (2021).
5. P. K. Wong, T. H. Wang, J. H. Deval, and C. M. Ho, "Electrokinetics in micro devices for biotechnology applications," IEEE/ASME Trans. Mechatron. **9**(2), 366–376 (2004).
6. K. Ahn, C. Kerbage, T. P. Hunt, R. M. Westervelt, D. R. Link, and D. A. Weitz, "Dielectrophoretic manipulation of drops for high-speed microfluidic sorting devices," Appl. Phys. Lett. **88**(2), 024104 (2006).
7. M. Abdelgawad and A. R. Wheeler, "The digital revolution: a new paradigm for microfluidics," Adv. Mater. **21**(8), 920–925 (2009).
8. A. R. Wheeler, "Putting electrowetting to work," Science **322**(5901), 539–540 (2008).
9. I. Barbulovic-Nad, H. Yang, P. S. Park, and A. R. Wheler, "Digital microfluidics for cell-based assays," Lab Chip **8**(4), 519–526 (2008).
10. K. Choi, A. H. C. Ng, R. Fobel, and A. R. Wheeler, "Digital microfluidics," Annu. Rev. Anal. Chem. **5**(1), 413–440 (2012).
11. A. Ashkin, J. M. Dziedzic, J. E. Bjorkholm, and S. Chu, "Observation of a single-beam gradient force optical trap for dielectric particles," Opt. Lett. **11**(5), 288 (1986).
12. P. Rodríguez-Sevilla, L. Labrador-Páez, D. Jaque, and P. Haro-González, "Optical trapping for biosensing: Materials and applications," J. Mater. Chem. **5**(46), 9085–9101 (2017).
13. P. Y. Chiou, A. T. Ohta, and M. C. Wu, "Massively parallel manipulation of single cells and microparticles using optical images," Nature **436**(7049), 370–372 (2005).
14. M. C. Wu, "Optoelectronic tweezers," Nat. Photonics **5**(6), 322–324 (2011).
15. D. R. Burnham and D. McGloin, "Holographic optical trapping of aerosol droplets," Opt. Express **14**(9), 4176–4181 (2006).

Biomedical Optics EXPRESS

16. D. McGloin, D. R. Burnham, M. D. Summers, D. Rudd, N. Dewar, and S. Anand, "Optical manipulation of airborne particles: techniques and applications," Faraday Discuss. **137**, 335–350 (2008).
17. A. Ashkin, J. M. Dziedzic, and T. Yamane, "Optical trapping and manipulation of single cells using infrared laser beams," Nature **330**(6150), 769–771 (1987).
18. A. I. Bunea and J. Glückstad, "Strategies for optical trapping in biological simples: aiming at microrobotic surgeons," Laser Photonics Rev. **13**(4), 1800227 (2019).
19. A. T. Ohta, P. Y. Chiou, T. H. Han, J. C. Liao, U. Bhardwaj, E. R. B. McCabe, F. Yu, R. Sun, and M. C. Wu, "Dynamic cell and microparticle control via optoelectronic tweezers," J. Microelectromech. Syst. **16**(3), 491–499 (2007).
20. . Zhang, N. Shakiba, Y. Chen, Y. Zhang, P. Tian, J. Singh, M. D. Chamberlain, M. Satkauskas, A. G. Flood, N. P. Kherani, S. Yu, P. W. Zandstra, and A. R. Wheeler, "Patterned optoelectronic tweezers: A new scheme for selecting, moving, and storing dielectric particles and cells," Small **14**(45), 1803342 (2018).
21. P. Y. Chiou, S. Y. Park, and M. C. Wu, "Continuous optoelectrowetting for picoliter droplet manipulation," Appl. Phys. Lett. **93**(22), 221110 (2008).
22. S. Y. Park, C. Pan, T. H. Wu, C. Kloss, S. Kalim, C. E. Callahan, M. Teitell, and P. Y. Chiou, "Floating electrode optoelectronic tweezers: Light-driven dielectrophoretic droplets manipulation in electrically insulating oil medium," Appl. Phys. Lett. **92**(15), 151101 (2008).
23. S. Y. Park, S. Kalim, C. Callahan, M. A. Teitell, and E. P. Y. Chiou, "A light-induced dielectrophoretic droplet manipulation platform," Lab Chip **9**(22), 3228–3235 (2009).
24. S. Y. Park, M. A. Teitell, and E. P. Y. Chiou, "Single-sided continuous optoelectrowetting (SCOEW) for droplet manipulation with light patterns," Lab Chip **10**(13), 1655–1661 (2010).
25. J. Villarroel, H. Burgos, A. García-Cabañes, M. Carrascosa, A. Blázquez-Castro, and F. Agulló-López, "Photovoltaic versus optical tweezers," Opt. Express **19**(24), 24320 (2011).
26. H. A. Eggert, F. Y. Kuhnert, K. Buse, J. R. Adleman, and D. Psaltis, "Trapping of dielectric particles with light-induced space-charge fields," Appl. Phys. Lett. **90**(24), 241909 (2007).
27. M. Carrascosa, A. García-Cabañes, M. Jubera, J. B. Ramiro, and F. Agulló-López, "$LiNbO_3$: A photovoltaic substrate for massive parallel manipulation and patterning of nano-objects," Appl. Phys. Rev. **2**(4), 040605 (2015).
28. A. García-Cabañes, A. Blázquez-Castro, L. Arizmendi, F. Agulló-López, and M. Carrascosa, "Recent achievements on photovoltaic optoelectronic tweezers based on lithium niobate," Crystals **8**(2), 65 (2018).
29. A. Puerto, J. F. Muñoz-Martín, A. Mendez, L. Arizmendi, A. García-Cabañes, F. Agulló-López, and M. Carrascosa, "Synergy between pyroelectric and photovoltaic effects for optoelectronic nanoparticle manipulation," Opt. Express **27**(2), 804–815 (2019).
30. M. Esseling, F. Holtmann, M. Woerdemann, and C. Denz, "Two-dimensional dielectrophoretic particle trapping in a hybrid crystal/PDMS-system," Opt. Express **18**(16), 17404–17411 (2010).
31. J. Matarrubia, A. García-Cabañes, J. L. Plaza, F. Agulló-López, and M. Carrascosa, "Optimization of particle trapping and patterning via photovoltaic tweezers: role of light modulation and particle size," J. Phys. D: Appl. Phys. **47**(26), 265101 (2014).
32. C. Sebastian-Vicente, E. Muñoz-Cortés, A. García-Cabañes, F. Agulló-López, and M. Carrascosa, "Real-time operation of photovoltaic optoelectronic tweezers: new strategies for massive nano-object manipulation and reconfigurable patterning," Part. Part. Syst. Charact. **36**(9), 1900233 (2019).
33. H. Burgos, M. Jubera, J. Villarroel, A. García-Cabañes, F. Agulló-López, and M. Carrascosa, "Role of particle anisotropy and deposition method on the patterning of nano-objects by photovoltaic effect in $LiNbO_3$," Opt. Mater. **35**(9), 1700–1705 (2013).
34. M. Jubera, A. García-Cabañes, J. Olivares, A. Alcazar, and M. Carrascosa, "Particle trapping and structuring on the surface of $LiNbO_3$:Fe optical waveguides using photovoltaic fields," Opt. Lett. **39**(3), 649–652 (2014).
35. A. Puerto, A. Méndez, L. Arizmendi, A. García-Cabañes, and M. Carrascosa, "Optoelectronic manipulation, trapping, splitting, and merging of water droplets and aqueous biodropltes based on the bulk photovoltaic effect," Phys. Rev. Appl. **14**(2), 024046 (2020).
36. M. Esseling, A. Zaltron, W. Horn, and C. Denz, "Optofluidic droplet router," Laser Photonics Rev. **9**(1), 98–104 (2015).
37. L. Chen, B. Fan, W. Yan, S. Li, L. Shi, and H. Chen, "Photo-assisted splitting of dielectric microdroplets in a LN-based sandwich structure," Opt. Lett. **41**(19), 4558–4561 (2016).
38. L. Chen, S. Li, B. Fan, W. Yan, D. Wang, L. Shi, H. Chen, D. Ban, and S. Sun, "Dielectrophoretic -behaviours of microdroplet sandwiched between LN substrates," Sci. Rep. **6**(1), 29166 (2016).
39. F. Li, X. Zhang, K. Gao, L. Shi, Z. Zan, Z. Gao, C. Liang, E. R. Mugisha, H. Chen, and W. Yan, "All-optical splitting of dielectric microdroplets by using a y-cut-LN-based anti-symmetrical sandwich structure," Opt. Express **27**(18), 25767–25776 (2019).
40. B. Fan, F. Li, L. Chen, L. Shi, W. Yan, Y. Zhang, S. Li, X. Wang, X. Wang, and H. Chen, "Photovoltaic manipulation of water microdroplets on a hydrophobic LiNbO3 substrate," Phys. Rev. Appl. **7**(6), 064010 (2017).
41. E. Muñoz-Cortés, A. Puerto, A. Blázquez-Castro, L. Arizmendi, J. L. Bella, C. López-Fernández, M. Carrascosa, and A. García-Cabañes, "Optoelectronic generation of bio-aqueous femto-droplets based on the bulk photovoltaic effect," Opt. Lett. **45**(5), 1164–1167 (2020).

Biomedical Optics EXPRESS

42. Z. Gao, Y. Mi, M. Wang, X. Liu, X. Zhang, K. Gao, L. shi, E. R. Mugisha, H. Chen, and W. Yan, "Hydrophobic-substrate based water-microdroplet manipulation through the long-range photovoltaic interaction from a distant $LiNbO_3$:Fe crystal," Opt. Express **29**(3), 3808–3824 (2021).
43. F. Agulló-López, G. F. Calvo, and M. Carrascosa, *Photorefractive Materials and Their Applications*, 113P. Günter and J. P. Huignard, eds. (Springer, 2006), pp. 43–82.
44. J. F. Muñoz-Martínez, I. Elvira, M. Jubera, A. García-Cabañes, J. B. Ramiro, C. Arregui, and M. Carrascosa, "Efficient photo-induced dielectrophoretic particle trapping on Fe:$LiNbO_3$ for arbitrary two dimensional patterning," Opt. Mater. Express **5**(5), 1137–1146 (2015).
45. T. B. Jones, *Electromechanics of Particles* (Cambridge University, 1995).
46. X. Zhang, J. Wang, B. Tang, X. Tan, R. A. Rupp, L. Pan, Y. Kong, Q. Sun, and J. Xu, "Optical trapping and manipulation of metallic micro/nanoparticles via photorefractive crystals," Opt. Express **17**(12), 9981–9988 (2009).
47. P. Mokrý, M. Marvan, and J. Fousek, "Patterning of dielectric nanoparticles using dielectrophoretic forces generated by ferroelectric polydomain films," J. Appl. Phys. **107**(9), 094104 (2010).
48. C. M. Phan, B. Allen, L. B. Peters, T. N. Le, and M. O. Tale, "Can water float on oil?" Langmuir **28**(10), 4609–4613 (2012).
49. C. M. Phan, "Stability of a floating water droplet on an oil Surface," Langmuir **30**(3), 768–773 (2014).
50. S. A. Basun, D. R. Evans, T. J. Bunning, S. Guha, J. O. Barnes, G. Cook, and R. S. Meltzer, "Optical absorption spectroscopy of Fe^{2+} and Fe^{3+} ions in $LiNbO_3$," J. Appl. Phys. **92**(12), 7051–7055 (2002).
51. A. C. Nevo, I. Michaeli, and H. Schindler, "Electrophoretic properties of bull and of rabbit spermatozoa," Exp. Cell Res. **23**(1), 69–83 (1961).
52. M. Skoda, K. Hiromi, and K. Akasaka, "Kinetic studies of interaction between acridine orange DNA," Biopolymers **10**(6), 1003–1012 (1971).